Physical and Clinical Evaluation of High-Resolution Thyroid Pinhole Tomography

Patrick M. Wanet, Alain Sand and Jean Abramovici
De Bijloke Hospital, Ghent, van Helmont Hospital, Vilvoorde and H. Familie Hospital, Reet, Belgium

High-resolution pinhole-SPECT (PSPECT) is a new method for examining the thyroid gland. **Methods:** The camera is tilted slightly so that it is as close to the thyroid as possible. Patients are injected with 185–260 MBq (5–7 mCi) of [^{99m}Tc]pertechnetate and examined for 20 min. The reconstruction algorithm is based on filtered backprojection. **Results:** We performed static scintigraphy on the thyroids of 114 patients, followed by PSPECT. The major advantage of P SPECT is high resolution. Three- and 4-mm-pinholes produce resolutions of 6 mm and 7 mm, respectively, while resolutions obtained with a parallel collimator are always above 15 mm. The second advantage associated with this method is the good visualization of the cold nodules surrounded by higher activity. Finally, the reconstruction program provides exact sizes of thyroids. **Conclusion:** SPECT is a powerful tool for examining the thyroid.

Key Words: pinhole collimator; thyroid; SPECT

J Nucl Med 1996; 37:2017–2020

Normally, SPECT is performed using parallel-hole collimators. However, the spatial resolution achievable with these collimators is too low for some clinical applications. This applies to thyroid SPECT, which requires high spatial resolution. We developed a method by which thyroid tomography can be performed using pinhole collimators. This method offers a good compromise in terms of resolution, sensitivity and reconstruction time.

There are only a few published papers concerning pinhole single-photon emission computed tomography (PSPECT). Most of these report on nonclinical work or applications in small animals (*1–2*). Multipinhole collimation has also been investigated for a small field of view (*3–4*). SPECT imaging of the thyroid using slant-hole collimators has also been investigated. However, this method cannot reliably detect hypofunctioning nodules having diameters less than 1.5 cm (*5*). Preliminary clinical studies on PSPECT have been published over the last few years (*6–9*).

We used a rotating single-head gamma camera equipped with a pinhole collimator. We tilted the camera so that the distance between the pinhole aperture and the thyroid gland was reduced. We used a modified cone-beam algorithm to reconstruct the PSPECT images. We evaluated reconstruction on phantom studies and normal volunteers. Tomographic slices were compared with static acquisition and echography. We performed thyroid PSPECT on 114 patients. In addition, we performed a complete examination of the thyroid. We present results from selected patients here.

MATERIALS AND METHODS

Acquisition

Patients were injected with 185–260 MBq (5–7 mCi) [^{99m}Tc]-pertechnetate. Static scintigraphy was performed 20 min after injection, followed by pinhole tomography. The camera was tilted in such a manner that the distance between the center of rotation and the collimator was reduced (Fig. 1).

Images were obtained under the following conditions:

Pinhole aperture size: 3 or 4 mm
Pixel resolution: 128 × 128, zoom 2
Camera rotation: 180° (starting from right lateral position and ending at the left lateral position)
Time per step: 20 to 30 sec
Total number of steps: 30 to 60.

Image quality was acceptable from 300 Kcounts and excellent from 500 Kcounts.

Reconstruction

Reconstruction was executed using a cone-beam algorithm. Our method was based on studies by Manglos et al. (*10*) and executed in four steps:

1. The acquisition frames were corrected for field nonuniformity.
2. The tilted-angle projections measured were transformed into a set of virtual nontilted projections (Fig. 2).
3. The corrected projections were filtered along a perpendicular axis to the axis of rotation of the camera and are subsequently backprojected according to Manglos' algorithm (*10*). Since the thyroid gland is relatively small, no distortions were observed in the reconstructed images. Thus, this method offers a good compromise between quality and reconstruction speed.
4. The transaxial slices were used to reconstruct the coronal slices and three-dimensional images.

We ran the program on a Elscint SPX computer (Elscint Ltd., Haifa, Israel). A transaxial slice was reconstructed in 2 sec.

Collimator Studies

Figure 1 shows three possible ways to perform thyroid tomography. When a parallel collimator is used, the distance between the center of rotation and the collimator face is around 25 cm. When the pinhole is used and the camera tilted, the distance can be reduced to approximately 8 to 10 cm. When the camera is not tilted, the distance is around 13 to 18 cm. An angle of 10° to 15° provides a good compromise between efficiency and reconstruction quality.

Figure 3 shows resolution as a function of the geometric efficiency in three different situations. These curves were calculated from the formulas given by Ott et al. (*11*). The lowest curve in Figure 3 shows the resolution and sensitivity for different kinds of pinholes (diameters of 1 to 6 mm). This curve was calculated for a distance of 9 cm.

The middle curve is valid when the camera is not tilted. The top curve was obtained for different kinds of parallel collimators. A low-energy, high-resolution collimator (LEHR) produces a resolution of 16 mm and a geometrical efficiency that is comparable with

Received Oct. 5, 1995; revision accepted Mar. 6, 1996.
For correspondence or reprints contact: Patrick M. Wanet PhD, De Bijloke Ziekenhuis, Dienst Radioisotopen, H. Dunantlaan, 5, B-9000 Gent, Belgium.

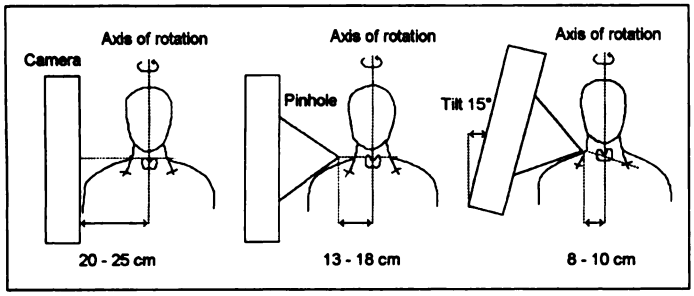

FIGURE 1. Position of the camera with a parallel collimator (left), a nontilted pinhole collimator (middle) and a tilted pinhole collimator (right). Because of the shorter distance between the pinhole and the thyroid, both resolution and sensitivity increase.

that of a 4-mm pinhole. However, when a 4-mm pinhole is used, a resolution of 7 mm can be obtained.

RESULTS

Phantom Studies

Figures 4 and 5 show the thyroid phantom used to test our reconstruction program. This phantom was filled with 37 MBq ^{99m}Tc. Tomographical images were obtained using a rotating scintillation camera (Elscint SP6) equipped with a 4-mm pinhole. Sixty projections were collected over 30 min. The coronal slices (Fig. 6A) clearly show the two levels of activity inside the phantom. The three-dimensional views (Fig. 6B) show the phantom as it is represented in Figure 5. These views were calculated with a 30% threshold. The size of both lobes and the largest nodules can be determined. The smallest nodule (6 mm) can be detected visually but not measured.

Another acquisition was performed on this phantom, filled with the same activity and over the same period. We used a single-head camera equipped with a high-resolution collimator. This collimator was placed 25 cm from the center of rotation to simulate real acquisition. The coronal slices are shown in Figure 6C. These should be compared with Figure 6A. The differences between these demonstrate the superiority of PSPECT.

Patient Studies

We used a LEHR parallel collimator and a 4-mm pinhole with and without tilt to perform three tomographic examinations on a healthy volunteer. The counting rates were 0.58 (LEHR), 0.57 (pinhole with tilt) and 0.28 Kcount/sec (pinhole without tilt), respectively.

The transaxial and coronal slices after a tilted pinhole acquisition are shown in Figures 7A and 7B. Figure 7C shows

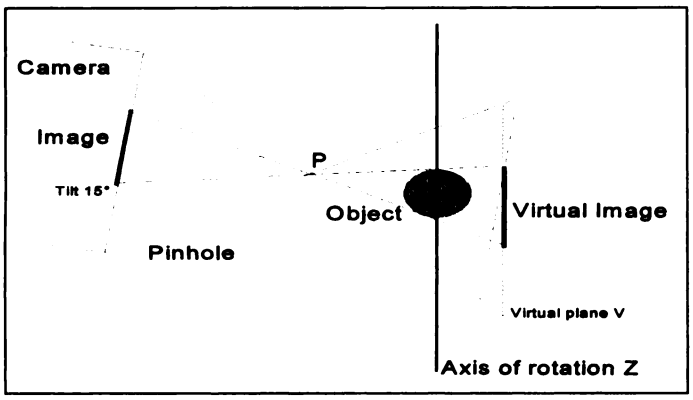

FIGURE 2. View of the tilt-angle geometry. The object is located on the axis of rotation. An image is projected on the crystal through the pinhole, P. A virtual image is calculated on the virtual plane, V. This image is convergently backprojected in the direction of the pinhole, P.

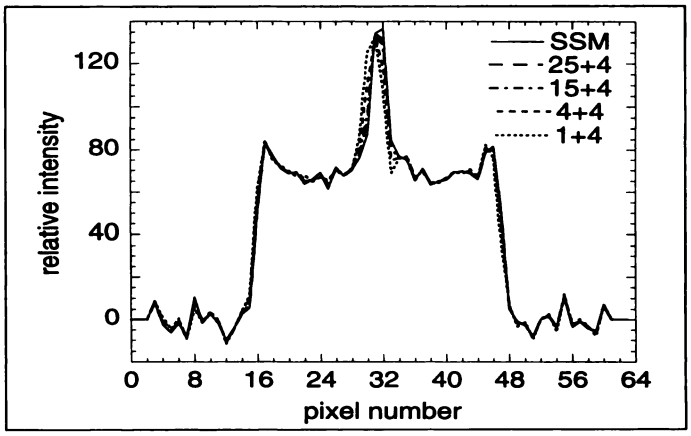

FIGURE 3. Spatial resolution (FWHM in mm) plotted as a function of geometrical efficiency compares parallel collimators (distance d = 25 cm) and pinhole collimators with (d = 9 cm) and without tilt (d = 13 cm).

anterior and posterior three-dimensional surface views. The height of the right and left lobe is 6.0 cm and 5.0 cm, respectively. The three-dimensional views were calculated after a 30% background substraction. These values are in good agreement with those found by MRI (6.4 and 6.5 cm, respectively). Figure 7D shows the two sagittal slices and the sagittal MRI views.

We included 114 patients in this study (25 men, 89 women; mean age: 54.9 yr, range 17–95 yr). No tomographic examination was performed on 11 patients (9.6%) because the counting rate was too low. Tomography was not performed when the total count was below 300 kcts. Static scintigraphy and tomography of 21 patients were normal. Of the 82 pathological patients, we found discrepancies between the static and tomographic results of 15 patients (18%). All of these discrepancies were confirmed by echography. In the other patients, tomography confirmed the static scintigraphic findings. However, elevated contrast allowed easier diagnosis.

Tomographic findings do not agree with static scintigraphic findings in 18% of our pathological cases. This is observed in the following three cases. Figure 8A shows an extremely heterogenous static view. The coronal slices show a cold and a hot nodule in the right lobe (Fig. 8B). They are located on the same transaxial slice. They have a diameter of approximately 12 mm. (Fig. 8C). Figure 8D shows the echography on the same level. The diameters of the two nodules are 11.8 mm and 12.5 mm, respectively.

The second case illustrates a complete discrepancy between

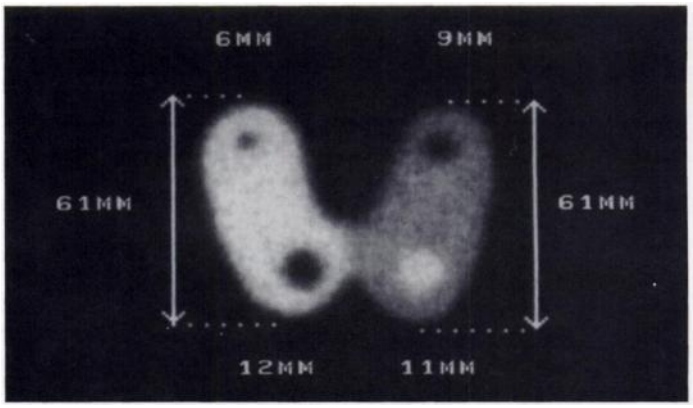

FIGURE 4. Thyroid phantom filled with ^{99m}Tc static scintigraphy. There are two levels of activity in the ratio 1:2. The diameters of the three cold spots are 6, 9 and 12 mm. There is also a hot spot of 11 mm. The height of each lobe is 6.1 cm.

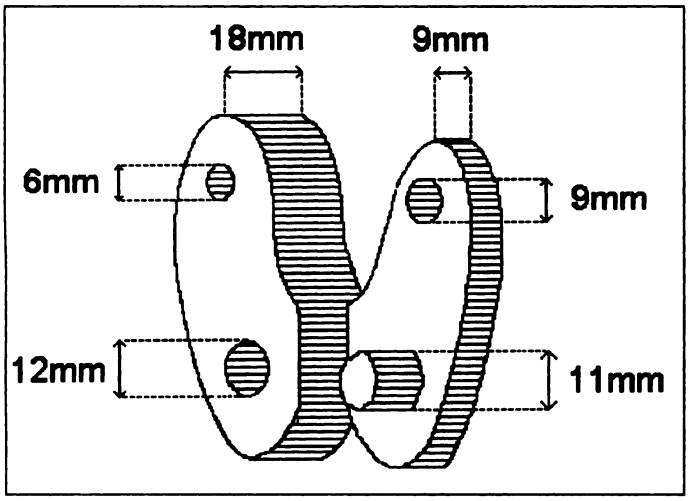

FIGURE 5. Diagram of the thyroid phantom showing the three-dimensional repartition of the activity. Right oblique posterior view.

static and tomographic acquisition. The static findings is normal (Fig. 9A), but the coronal slices show a cold nodule, (Fig. 9B) that is also visible on the three-dimensional views (Fig. 9C). Echography confirmed a nodule of 20 × 21 mm, slightly larger than that measured by us. Such false-negative results from static scintigraphy are not unusual and demonstrate the superiority of PSPECT.

On the other hand, static scintigraphy sometimes exhibits areas of lower activity, suggesting the presence of a cold nodule (Fig. 10A). The three-dimensional views show that the right part of the right lobe is slightly thinner than the rest of the thyroid gland giving a false impression of cold nodule on the static scintigraphy (Fig. 10B). The echography of this patient is normal.

CONCLUSION

This article describes a thyroid tomography procedure using a pinhole collimator. The camera is tilted to reduce the distance between the pinhole and the center of rotation. Geometric efficiency increases by a factor of two and resolution is improved by 3 mm.

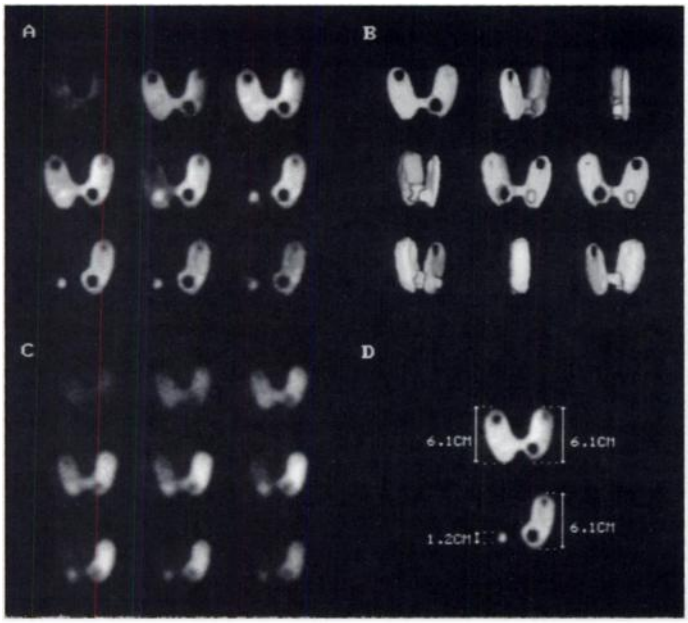

FIGURE 6. Thyroid phantom: (A) coronal slices after acquisition with a 4-mm pinhole. (B) Three-dimensional reconstruction views. (C) Coronal slices after acquisition with a single-head camera equipped with a LEHR collimator. (D) Lower and upper levels with measurements.

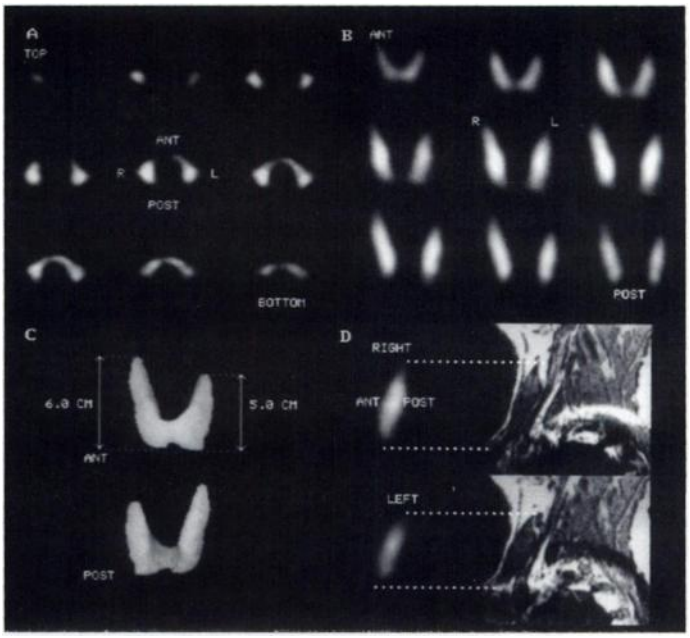

FIGURE 7. Volunteer study: (A) transaxial slices after acquisition with a 4-mm pinhole. (B) Coronal slices. (C) Three-dimensional reconstruction views. (D) Sagittal and NMR views.

Reconstruction is based on a method described by Manglos et al. (*10*). It offers a good compromise between reconstruction time and accuracy. Filtered backprojection is limited. However, image quality is sufficiently accurate for clinical application. We examined 114 patients. We have only performed static scintigraphy on patients because the counting rate was too low to perform tomography under good conditions. To guarantee sufficient quality of tomography, the total count must always be greater than 300 kcts.

High resolution is the major advantage offered by PSPECT. Pinholes with diameters of 3 and 4 mm provide resolutions of 6 and 7 mm, respectively. Resolution obtained with a parallel collimator is rather low, providing insufficient tomographic quality. This can be attributed to the fact that the distance

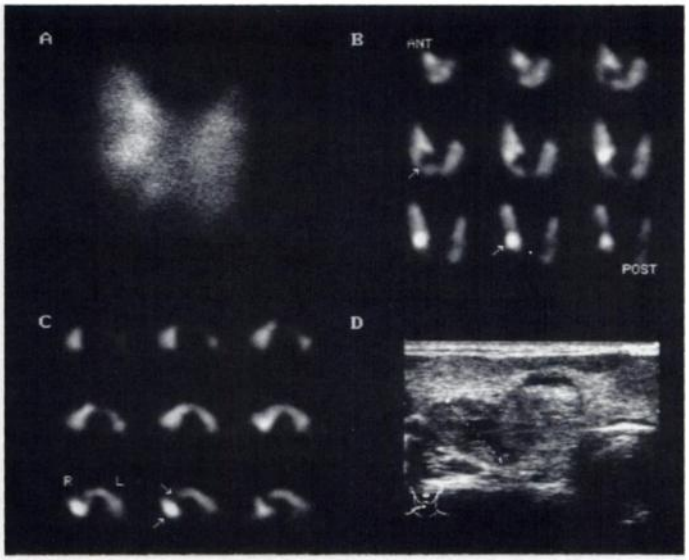

FIGURE 8. (A) Static scintigraphy. (B) Coronal slices clearly showing the two nodules. (C) Transaxial slices, with the two nodules visible on Slices 7 and 8. (D) Echography performed on the same level as Slice 7.

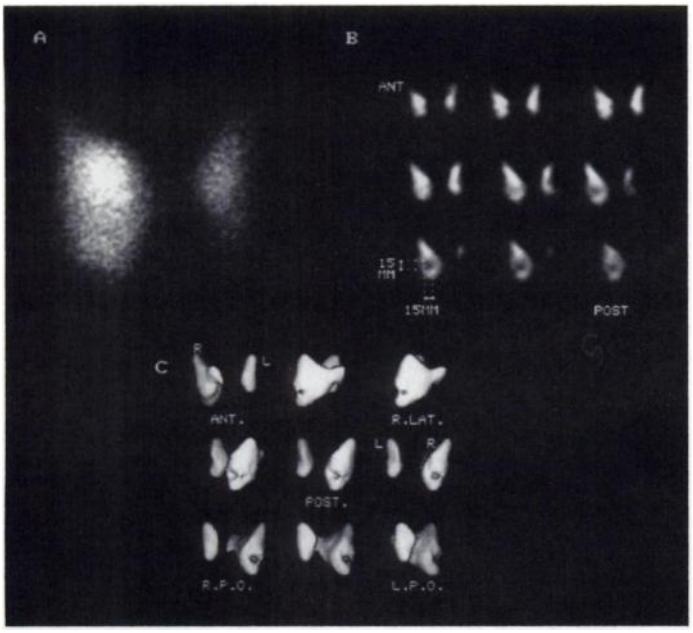

FIGURE 9. (A) Normal static scintigraphy. (B) Coronal slices showing a cold nodule (15 × 15 mm) in the right lobe. (C) Three-dimensional views clearly showing the posterior position of the cold nodule.

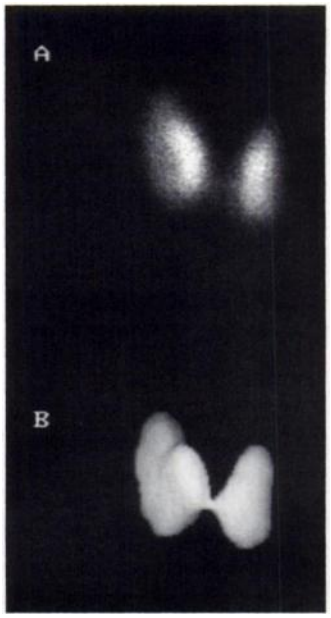

FIGURE 10. (A) Static scintigraphy with an area of decreased activity in the right lobe. (B) Normal three-dimensional view.

between collimator and center of rotation cannot be reduced below 20 to 25 cm due to the patients' shoulders.

Second, thyroid tomography in particular can be used to detect cold nodules surrounded by higher activity which are located posteriorly. Figure 9 illustrates this. We observed a total contradiction between static scintigraphic and tomographic findings in a few patients. Figure 9 illustrates this well. Nevertheless, in many patients, particularly those with multinodular goiters, tomography only confirms the findings of the static view. However, tomographic pictures are more precise.

The third advantage of PSPECT is that the thyroid gland can be measured. For large nodules (>2 cm), there is good agreement between echography and tomography. Because of the resolution in tomography (between 6 and 7 mm), nodules smaller than 1 cm could not be measured. Five-millimeter nodules can be detected visually on the coronal slices.

This method has also been tested on cervical spine tomography. The counting rate is too low and clinical imaging time is unacceptable. The use of PSPECT in bone applications is being investigated. PSPECT is a powerful tool for thyroid examination.

ACKNOWLEDGMENTS

We thank Prof. De Roose of UZ Gent, Belgium, Drs. Hermanus and Nijboer of Radiology and Surgery, van Helmont Ziekenhuis, Vilvoorde, Belgium, and Dr. H. Claes of Radiology, Vilvoorde, Belgium for providing imaging studies. We particularly thank Dr. G. Muret of Dinant Hospital, Regional Hospital, Namur, Belgium for MRI and echography support. We are also grateful to J. Behets of Elscint Benelux, Zaventem, Belgium, to M. Wilk, A. Soil, A. Peretz, N. Hermony of Elscint Ltd., Haïfa, Israel for useful discussions about implementing the Elscint camera software, and to I. Mindel for editorial assistance.

REFERENCES

1. Palmer J, Wollmer P. Pinhole emission computed tomography: method and experimental evaluation. *Phys Med Biol* 1990;35:339–350.
2. Weber DA, Ivanovic M, Franceschi D, et al. Pinhole SPECT: an approach to in vivo high-resolution SPECT imaging in small laboratory animals. *J Nucl Med* 1994;35: 342–348.
3. Jaszczak RJ, Li J, Wang H, Zalutsky R, Coleman RE. Pinhole collimation for ultra-high resolution, small field-of-view SPECT. *Phys Med Biol* 1994;39:425–437.
4. Li J, Jaszczak RJ, Wang H, Coleman RE. Multipinhole collimation for super-high resolution, small field-of-view SPECT [Abstract]. *J Nucl Med* 1994;35:27P.
5. Chen JJ, LaFrance ND, Allo MD, Cooper DS, Ladenson PW. SPECT of the thyroid. *J Clin Endocrinol Metab* 1988;66:1240–1246.
6. Olsson LE, Ahlgren L. Tomographic scintigraphy using a pinhole collimator and a rotating gamma camera. *Nuklearmedizin* 1990;29:47–50.
7. Wanet P, Stegen M, Sand A, Abramovici J. High-resolution pinhole SPECT of the thyroid: method and clinical evaluation [Abstract]. *Eur J Nucl Med* 1994;21:794.
8. Wanet P, Sand A, Abramovici J. High-resolution pinhole SPECT of the thyroid: clinical evaluation after one year experience [Abstract]. *Eur J Nucl Med* 1995;22:745.
9. Stegen M, Wanet P, Metello L, Rubinstein M. Improving sensitivity of thyroid scintigraphy using pinhole SPECT [Abstract]. *Eur J Nucl Med* 1995;22:745.
10. Manglos SH, Jaszczak RJ, Greer KL. Cone beam SPECT reconstruction with camera tilt. *Phys Med Biol* 1989;34:625–631.
11. Ott RJ, Flower MA, Babich JW, Marsden PK. *The physics of radioisotope imaging*. In: Webb S. eds *The physics of medical imaging*. Bristol: Adam Hilger 1988:143–181.